Advances and Applications in Bioinformatics and Chemistry

Dovepress

open access to scientific and medical research

Open Access Full Text Article

ORIGINAL RESEARCH

Simultaneous use of solution, solid-state NMR and X-ray crystallography to study the conformational landscape of the Crh protein during oligomerization and crystallization

This article was published in the following Dove Press journal:
Advances and Applications in Bioinformatics and Chemistry
4 June 2010
Number of times this article has been viewed

Benjamin Bardiaux[1,6]
Adrien Favier[2]
Manuel Etzkorn[4]
Marc Baldus[5]
Anja Böckmann[3]
Michael Nilges[1]
Thérèse E Malliavin[1]

[1]Unité de Bioinformatique Structurale, CNRS URA 2185, Institut Pasteur, Paris, France; [2]Institut de Biologie Structurale Jean-Pierre Ebel CEA-CNRS-Université Joseph Fourier, Grenoble, France; [3]Institut de Biologie et Chimie des Proteines, UMR 5086 CNRS/Université de Lyon 1, Lyon, France; [4]Max Planck Institute Biophysical Chemistry, Göttingen, Germany; [5]Bijvoet Center for Biomolecular Research Faculty of Science, Utrecht University Utrecht, The Netherlands; [6]Campus Berlin-Buch, Berlin, Germany

Abstract: We explore, using the Crh protein dimer as a model, how information from solution NMR, solid-state NMR and X-ray crystallography can be combined using structural bioinformatics methods, in order to get insights into the transition from solution to crystal. Using solid-state NMR chemical shifts, we filtered intra-monomer NMR distance restraints in order to keep only the restraints valid in the solid state. These filtered restraints were added to solid-state NMR restraints recorded on the dimer state to sample the conformational landscape explored during the oligomerization process. The use of non-crystallographic symmetries then permitted the extraction of converged conformers subsets. Ensembles of NMR and crystallographic conformers calculated independently display similar variability in monomer orientation, which supports a funnel shape for the conformational space explored during the solution-crystal transition. Insights into alternative conformations possibly sampled during oligomerization were obtained by analyzing the relative orientation of the two monomers, according to the restraint precision. Molecular dynamics simulations of Crh confirmed the tendencies observed in NMR conformers, as a paradoxical increase of the distance between the two β1a strands, when the structure gets closer to the crystallographic structure, and the role of water bridges in this context.

Keywords: structural bioinformatics, NMR structure calculation, ARIA, non-crystallographic symmetry, crystallographic ensemble refinement, molecular dynamics simulation

Introduction

Solid-state NMR is aiming at structure elucidation of insoluble proteins, eg, membrane proteins, cytoskeletal proteins and protein fibrils, which form multimeric or polymeric protein assemblies, as viroporins,[1] light-harvesting complexes,[2] phospholamban,[3] or more complex interactions including soluble and insoluble protein fragments, as prion protein,[4] Het-s,[5] the human prion protein[6] or Ure2p.[7] The structural study of the monomeric soluble part can be carried out by solution NMR, in aqueous solution or in detergents, and the combined use of restraints from solution NMR, and of information, only accessible from solid-state NMR, about the oligomerization state, would be of great use to analyze the protein conformational landscape during the transition between the monomeric and multimeric states. Indeed, the joint use of solution and solid-state NMR recently revealed structural aspects of the αB-crystalline oligomer[8] and permitted the determination of phospholamban topology in membrane.[9]

We use as a model the *Bacillus subtilis* Crh protein (catabolite repression HPr), a phosphocarrier protein of the phosphoenolpyruvate: carbohydrate phosphotransferase system

Correspondence: Thérèse E Malliavin
Unité de Bioinformatique Structurale, CNRS URA 2185, Institut Pasteur 25-28 rue du Dr Roux, F-75724 Paris Cedex 15, France
Tel (33) 1 40 61 34 75
Fax (33) 1 45 68 87 19
Email terez@pasteur.fr

(Figure 1), which displays a large conformational variability. Its monomeric structure was determined in solution by solution NMR[10] (PDB entry: 1k1c) and is close to the HPr structure.[11–14] A conformational exchange between a monomeric and a dimeric structure was observed in solution, but selective precipitation of the dimeric protein hampered dimer structure determination.[15] The dimeric structure was then determined in the crystalline form by X-ray crystallography[16] (PDB entries: 1mo1, 1mu4), as well as from micro-crystals by ssNMR[17] (PDB entry: 2rlz). The transition from the monomeric to the dimeric form consists in the 3D domain swapping of strand β1 (Figure 1B, C). In the crystal, the dimers are interacting two-by-two to form a dimer of dimers. The wealth of structural information available for this protein, and its conformational variability make Crh a unique model to evaluate the feasibility of structure determination for multimeric proteins, using a mixed set of solution and ssNMR restraints and chemical shifts.

An additional aspect investigated concerns the relative orientation of the Crh monomers during the transition from solution to crystal. Getting structural information about such a transition is rare and could be of great value to understand the crystallization process of proteins. In that respect, ssNMR recently provided the opportunity to obtain information about starting points of crystallogenesis.[18]

In the present study, we focused on the calculations of Crh dimers and dimers of dimers, which represent well-documented conformations of the protein.[16] Based on the observation that Crh in solution undergoes a monomer/dimer equilibrium, we make the hypothesis that the dimeric state of Crh represent an initial stage of the crystal formation. In that frame, the dimer of dimers corresponds to later stages of the crystallogenesis.

Three series of NMR conformer generation were performed with a version of ARIA 2.2[19] dedicated to ssNMR. The first series used precise distance restraints determined on the X-ray crystallographic structure. The two last series explore the conformational landscape of Crh dimers during the oligomerization and the crystal formation. The sets of ARIA conformers are compared to molecular dynamics (MD) simulations starting from crystallographic structures of the Crh dimer and dimer of dimers. We observe a good convergence of the monomers, and a large variability of their relative orientation into the dimer. This variability is reduced by the application of non-crystallographic symmetry restraints. The variation of relative orientation of one monomer with respect to the other is maximum along the dimer longitudinal axis, in all conformations generated: (i) by ARIA, (ii) during molecular dynamics simulations, and (iii) in a crystallographic ensemble refinement[20] along structure factors. A balance between protein–water and protein–protein interaction plays a crucial role in the stabilization of the monomer orientation observed in the crystal.

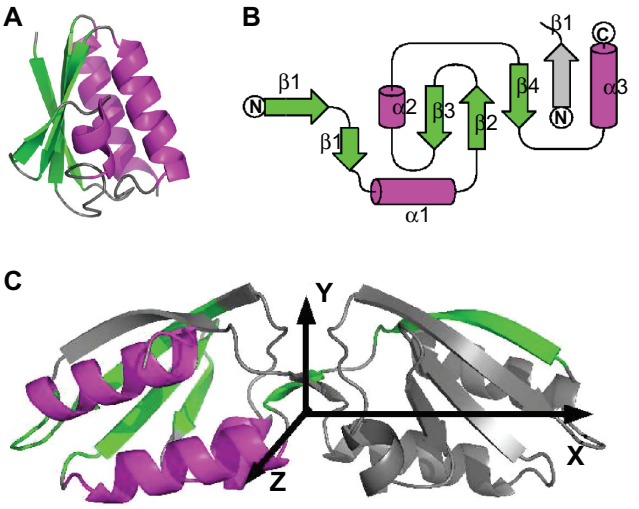

Figure 1 Structures of the Crh protein. **A**) The monomer structure determined by solution NMR (PDB entry: 1k1c) contains three α helices (α1: residues 17–28, α2: residues 47–50 and α3: residues 70–83) as well as a β sheet formed from four β strands (β1: residues 3–9, β2: residues 31–37, β3: residues 40–42 and β4: residues 60–67). **B**) Topology of a Crh monomer, inside the dimer, **C**) Dimer structure determined by X-ray crystallography (PDB entry: 1mo1). The β strands are in green and the α helices in magenta. In the dimer (b,c), one monomer is colored and the other one displayed in gray. In c, the axes X, Y, Z allowing to define the angles Ψ, Θ and Φ are drawn. This figure was realized with pymol 0.98[51] and TopDraw.[52]

Materials and methods

Input files of the conformers calculations

The NMR assignments of Crh in solution[10] and in the crystal[21] were obtained from the BMRB[22] (ids: 4972 and 5757). Inter-monomer assigned cross-peaks measured on the NHHC spectrum[23] were also used. The monomeric structure (PDB entry: 1k1c)[10] and the corresponding restraint file provided a synthetic NMR peak list for the monomer. The ψ and ϕ dihedral angle restraints were determined from TALOS version 2003.027.13.05,[24] using the ssNMR chemicals shifts (BMRB id: 5757). This prediction yields 26 hydrogen bonds in α-helices and 45 ϕ/ψ restraints in α-helices and β-strands. The accuracy of the conformers was analyzed with respect to two crystallographic structures[16] (PDB entries: 1mo1, 1mu4).

ARIA-CNS calculation

An iterative ARIA 2.2[19] calculation was used to filter the monomer NMR restraints using the ssNMR chemical shifts: eight iterations in geometric force field were performed starting from the synthetic monomer peak list and the ϕ, ψ dihedral restraints described in "Input files of the conformers

calculations". The other ARIA calculations (Figure 2) were based on a single iteration in geometric force field, generating 360 conformations. The calculations are performed on symmetric homodimers, and the dimer symmetry is enforced by minimizing the RMSD between monomer conformations, and ambiguous distance restraints (ADRs) are applied between the monomers.[25] A packing restraint to keep both monomers close in the 3D space is applied between the centers of mass, and is reduced from 15 to 0 kcal/mol.Å^2 during the protocol.

During the iterative calculation, ARIA assigns NOE cross-peaks in the following way. First, all possible assignments are derived for each peak by matching a list of chemical shifts with frequency windows centered around the position of a peak. Peak volumes are converted into distance restraints by using the isolated spin pair approximation, which relates the volume to the inverse sixth power of the distance between the two interacting spins. Ambiguous assignments are converted into ADRs, so that all assignment possibilities contribute to the target distance. Since most of the assignments are inconsistent, ARIA performs an iterative protocol to identify wrong assignments and noise peaks: at each iteration, the restraint list is corrected by filtering out unlikely assignments and noise peak, and then, based on the filtered restraint list, a new structure ensemble is calculated. This ensemble is analyzed in the next iteration. To compensate for the simplified treatment of non-bonded forces and missing solvent contacts during structure calculation, at the end of the iterative protocol, the conformers are further refined in explicit water to remove possible artifacts.[26]

During each iteration of the iterative or non iterative calculation, each protein conformer is produced by a simulated annealing procedure,[27] comprising: (i) high temperature torsion angle molecular dynamics (MD), (ii) torsion angle MD cooling phase, (iii) Cartesian space MD cooling phase using an increased number of steps (50,000 to 100,000 steps).[28]

The 50 lowest-energy conformers were then submitted to a geometric force field refinement with non-crystallographic symmetry (NCS) restraints and analyzed afterward by two clustering methods. The NCS restraints were applied

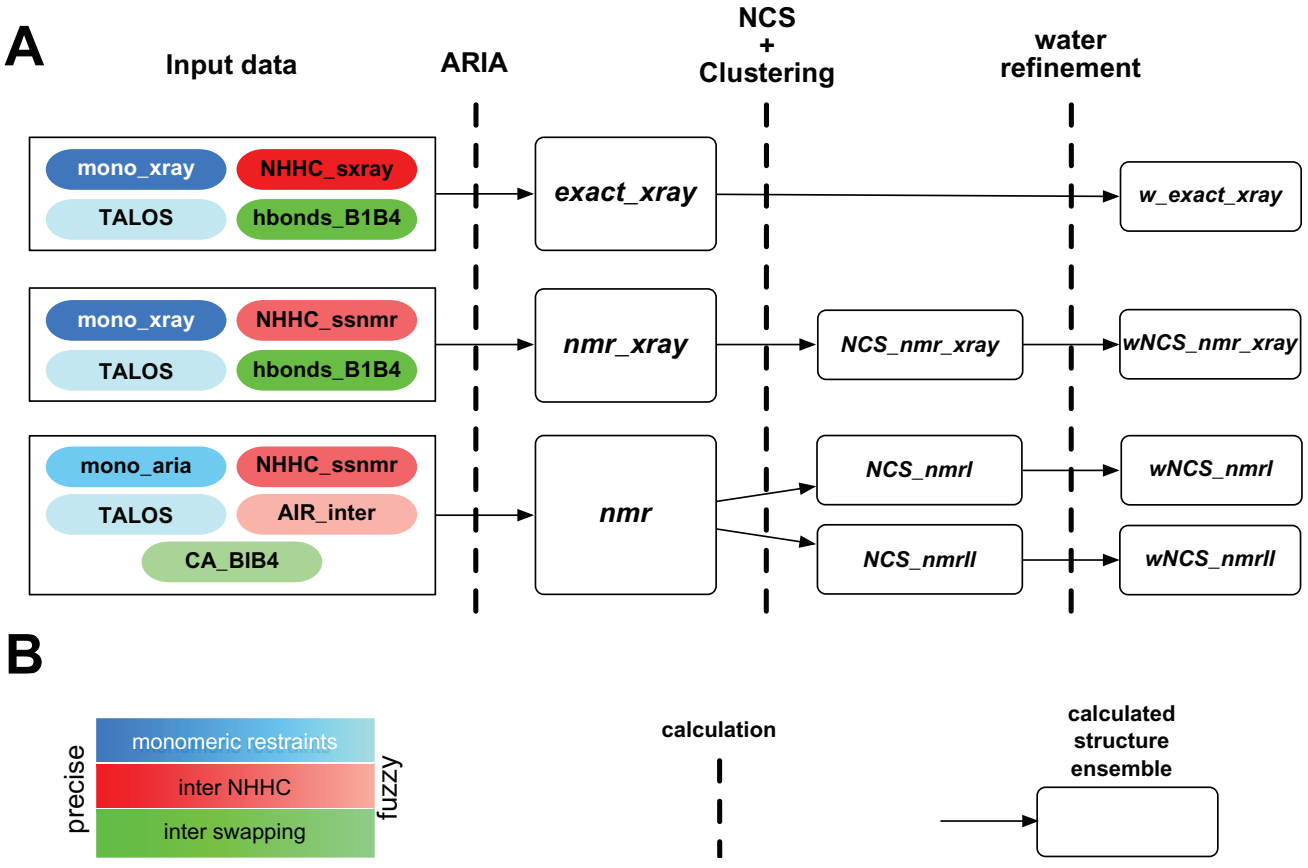

Figure 2 A) Scheme of the ARIA calculations. The colored boxes on the left describe the input data, the blue denoting intra-monomer restraints, the red denoting inter-monomer restraints coming from the interpretation of the ssNMR NHHC spectrum, the green denoting restraints of the swapping topology. The dark colors stand for precise crystallographic restraints, whereas light colors stand for fuzzy restraints originating from NMR measurements. The dashed vertical lines correspond to the calculation or to the processing of conformers, and the sets of conformers are given inside the white rectangles. **B**) Visual legend of (a).

between the dimers associated in the dimer of dimers using a strict relationship[29] based from the transformation (rotation and translation) between the two dimers in 1mo1. A water refinement with NCS restraints, including Lennard-Jones and electrostatic Coulombic potential was then performed on the resulting clusters.

Structure analysis

The RMSD between the backbone atoms was calculated by superimposing[30] residues 1–85 for the dimers, and residues 15–85 for the monomers. The fit to experimental restraints is evaluated from the number of violated distance restraints and the RMS of violations, a restraint being violated if the distance is larger than $U + 0.5\text{Å}$ or smaller than $L - 0.5\text{Å}$, where U and L are restraint upper and lower bounds. The conformers quality was analyzed by PROCHECK v.3.5.4[31] and WHATIF 5.1.[32]

The relative monomer orientation was described by the distance between the monomers centers of mass and by the Euler angles Ψ, Θ and Φ of the rotations describing the transformation from one monomer to the other. The rotation axes X, Y, Z are aligned along the principal inertia axes of the structure 1mu4 (Figure 1C).

The variation of Crh tertiary structure was monitored by calculating the minimum distances between axes of secondary structure elements. In the α-helices the axes are determined from the middles of the backbone atom segments (N(i), N(i+2)), (Cα(i), Cα (i+2)) and (C'(i), C'(i+2)), where *i* is the residue number. In the β strands, the axes are defined from the positions of backbone heavy atoms.

Clustering algorithms

Two algorithms were used to cluster the molecular conformations independently of the knowledge of the crystallographic structure. The first algorithm (clustering-I) similar to the one used in HADDOCK,[33] is based on the iterative processing of the pairwise coordinates RMSD matrix, using a RMSD cutoff and a minimal cluster size. The conformers are sorted into clusters, the cluster having the largest size is removed from the conformer pool, and the algorithm is run again on the remaining conformations. The distance cutoff varies from 2 to 4 Å, by steps of 0.1 Å, and the minimal cluster size varies from 5 to 10 by steps of 1, a given conformation belonging generally to several clusters. The second algorithm (clustering-II) groups conformers in two dimensions (clusters I versus conformers), by two successive hierarchical clusterings (command hclust of R[34]), applied first on the conformer axis, and then on the cluster axis.

Molecular dynamics simulations

The X-ray crystallographic structure 1mo1[16] containing a Crh dimer of dimers (chains A, B, C, D) was used as the starting point for the molecular dynamics (MD) simulations. The simulations were performed with periodic boundary conditions: *sol_dimer* on the chains A and B, and *sol_tetra*, *cryst_tetra* on the chains A, B, C and D (Table 1). The simulations *sol_dimer* and *sol_tetra* intend to describe the behavior of the Crh dimer and dimer of dimers in solution, whereas the simulation *cryst_tetra* models the Crh dimer of dimers in a more restricted environment, including qualitative crystal packing. A similar approach was used recently[35] to simulate proteins in the crystalline state.

The simulations *sol_dimer* and *sol_tetra* were performed at constant pressure, with a cutoff distance of 10 Å to determine the water box size. Conversely, the simulation *cryst_tetra* was performed at constant volume with a cutoff distance of 2 Å to determine the water box size, in order to model the effect of long-range order observed in the solid state. In *cryst_tetra*, the 10 sulfate molecules, and the 9 glycerol molecules observed in the crystal were kept in the simulation box.

Simulations of 10 ns were recorded using the package AMBER 9.0,[36] and the ff99SB force field.[37] A cutoff of 10 Å was used for Lennard-Jones interactions, and long-range electrostatic interactions were calculated with the Particle Mesh Ewald (PME) protocol.[38] The systems total charge was neutralized using sodium counterions ions. The SHAKE algorithm[39] was used to keep rigid all covalent bonds involving hydrogens, enabling a time step of 2 fs. Pressure was regulated with isotropic position scaling and a relaxation time of 1 ps, and temperature using a Langevin thermostat[40] with a collision frequency of 2 ps^{-1}. For *sol_dimer* and *sol_tetra*,

Table 1 Preparation details of the molecular dynamics simulations

	sol_dimer	*sol_tetra*	*cryst_tetra*
Number of counterions	6	12	32
Water box dimensions (Å)	74.1 × 89.7 × 58.3	72.5 × 91.7 × 81.1	58.9 × 79.2 × 68.9
Number of water molecules	9396	12560	6266
Total number of atoms	30918	43140	24454

the simulations were performed at temperature 298 K and pressure 1 atm, whereas for *cryst_tetra*, the temperature was 283 K, at which the ssNMR experiments[21] were recorded. Atom coordinates were saved every ps.

Simulations were initiated by some rounds of semi-restrained and then unrestrained minimization of the entire system. Heating of the system up to 300 K was realized during 20 ps at constant volume, while restraining the positions of the protein atoms with a force constant of 25 kcal/(mol.Å^2). The equilibration process was then performed: one MD round of 5 ps at constant volume and four MD rounds of 2.5 ps were run while reducing the position restraints from 25 kcal/(mol.Å^2) down to 5 kcal/(mol.Å^2); eventually a last MD round of 70 ps was performed with a restraint of 2.5 kcal/(mol.Å^2) to complete the system equilibration.

Ensemble crystallographic refinement

The Crh dimer of dimers was refined along the structure factors measured on 1mo1 (file: 1mo1-sf.cif). The ensemble crystallographic refinement,[20] generated 16 conformations of the oligomer, using CNS 1.2.[29] The starting conformation was the one observed in the PDB structure 1mo1. The water molecules and the cofactors (sulfate ions and glycerol) were not duplicated. Ten percents of the structure factors were used for data cross-validation. A R factor of 0.14 and a free R factor of 0.18 were observed on the set ens_XR.

Results

Filtering of the solution NMR restraints

The generation of oligomer conformations requires the use of intra-monomer restraints, and an objective method was used to filter among the solution NMR restraints observed for the Crh monomer, those still valid in the oligomer state observed by ssNMR. The filtering is based on ssNMR chemical shifts and provides restraints valid for microcrystalline as well as for precipitate states of Crh, as the same ssNMR spectrum was observed for both states.[41]

The possible interaction between β1 and β4 strands is formed very early during the protein oligomerization and crystallization, as it was observed from solution NMR chemical shifts.[10] Interactions between strands β1 and β4 were thus imposed through distance restraints corresponding to hydrogen bonds between the β strands, extracted from the X-ray crystallographic structure of Crh. Equivalent information about interaction interfaces could be obtained by mutational studies,[42] electron microscopy[43] or molecular dynamics simulations.[44,45]

An iterative ARIA calculation was performed on a symmetric homodimer to filter among the monomer NMR distance restraints, those still verified in the dimer structure. The inputs were: (i) the ssNMR sequential assignment of the Crh dimer,[21] (ii) the dihedral and intra-monomer hydrogen bond restraints deduced from the TALOS analysis of the ssNMR chemical shifts, (iii) the synthetic peak list built from the solution NMR distance restraints recorded on the residues 16–85. The synthetic peak list was submitted to ARIA along with the monomeric assignments in order to limit the number of restraint contributions and to consequently reduce the combinatorial analysis during the NOE assignment. The iterative ARIA run produced the mono_aria set of restraints. The contact map obtained from restraints mono_aria (Figure 3, lower triangle) is quite similar to the contact map of the restraints mono_xray obtained by filtering the 1k1c restraints directly on the crystallographic structure 1mo1 (Figure 3, upper triangle). The restraints mono_xray and mono_aria will be used as intra-monomer restraints during the ARIA calculations described below.

Presentation of ARIA calculations

Input restraints (Figure 2) include mono_aria and the TALOS restraints, described above, as well as the following inter-monomer restraints. Exact distances, measured on the structure 1mo1, for the inter-monomer peaks assigned on

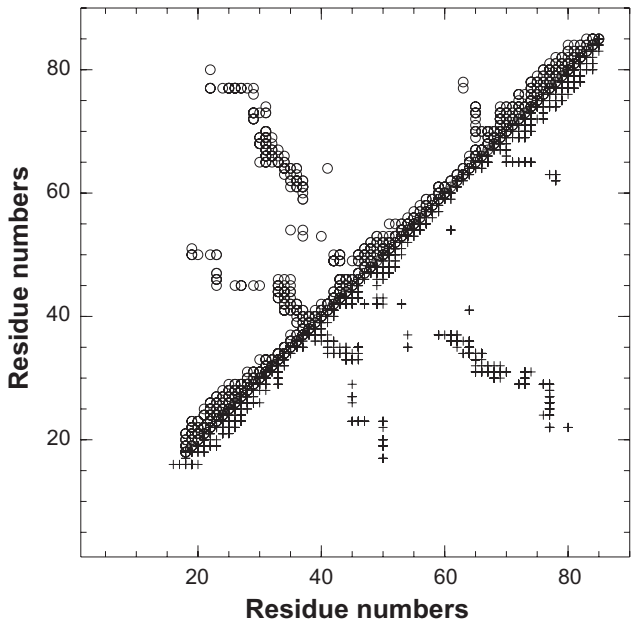

Figure 3 Comparison of the contact map obtained by filtering on the X-ray structure 1mo1 (upper triangle, empty circles) and of the contact map (restraints mono_aria) obtained by filtering monomer peak list using ssNMR chemical shifts (lower triangle, crosses). The restraints are plotted along the residue numbers.

the spectrum NHHC,[23] produce the restraints NHHC_xray. The NMR restraints NHHC_ssnmr are built from the NHHC peaks, using invariant bounds 2.5–4.5 Å. Additional inter-monomer restraints between the strands β1 and β4 were applied using hydrogen bond restraints (hbonds_B1B4) or using restraints 4.5–5.5 Å between Cα (CA B1B4), determined from 1mo1. Ambiguous inter-monomer restraints (AIR_inter) similar to the one used in HADDOCK[33] were applied between all residues assigned to the dimer interface by chemical shift perturbation in solution.[10]

Three sets of ARIA conformers were generated (Figure 2). The restraints used in the first conformer set (*exact_xray*) were: mono_xray, NHHC_xray, TALOS and hbonds_B1B4, based on exact crystallographic distances. This calculation was followed by a water refinement step (*w_exact_xray*). The second conformer set (*nmr_xray*) was obtained using a mixed set of ssNMR and crystallographic restraints: mono_xray, NHHC_ssnmr, TALOS and hbonds_B1B4, in order to explore the conformational landscape in presence of restraints close to those observed in the crystal. Finally, the third conformer set (*nmr*) was only based on NMR restraints (mono_aria, NHHC_ssnmr, TALOS) and on the information on dimerisation interface already observed in solution (CA_B1B4 and AIR_inter). This last conformer set intended to sample the conformational landscape of the Crh dimer of dimers during oligomerization and crystal formation. As no significant changes are observed between ssNMR spectra recorded on Crh micro-crystals and precipitates,[41] it is possible to assume that ssNMR restraints give information about the Crh oligomer architecture in the crystal as well as in the precipitate.

The study of Crh by NMR in solution[10] has shown that two modes of association are possible for the dimer, one arising via the swapping of the β1 strand. The crystallographic structure then gave the exact topology of the position of the strand β1.[16] The hypothesis made in the present work that the dimeric state of Crh represent an initial stage of the crystal formation, implies that the hydrogen bonds between β1 and β4, are formed early in the oligomerization process. The associated restraints, hydrogen bonds or restraints between the Cα bring a determinant information for the convergence of the relative monomer positions in the dimer.

The dimer conformations obtained from the sets *nmr_xray* and *nmr* were further refined using additional non-crystallographic symmetry (NCS) restraints in geometric force field, to produce the sets *NCS_nmr_xray* and *NCS_nmr*. The application of non-crystallographic symmetry (NCS) restraints represents only a qualitative short-range modeling of the crystal or precipitate order. An additional water refinement step was finally performed on a conformations cluster extracted from *NCS_nmr_xray* and on two clusters extracted from *NCS_nmr*, to produce the sets *wNCS_nmr_xray*, *wNCS_nmrI* and *wNCS_nmrII*. The sets *wNCS_nmrI* and *wNCS_nmrII* will be described more precisely in the section "Convergence of the calculation and fit to the NMR restraints".

Convergence of the calculation and fit to the NMR restraints

Clustering-I, described in Materials and Methods was performed on the 50 lowest-energy conformers calculated in the geometric force field (*exact_xray*, *nmr_xray* and *nmr*), and for the conformations of *NCS_nmr_xray* and *NCS_nmr*, calculated using NCS restraints. The number of clusters, the cluster sizes, the backbone precision inside the clusters and the accuracy to the X-ray structure 1mu4, were analyzed in Table 2. The six clusters detected for *exact_xray* and their larger sizes in the 38–45 range prove the calculation convergence. The slight decrease of the coordinate precision inside the clusters and of the accuracy to the structure 1mu4, as well as the appearance of 5-members clusters, reveal a decrease of the convergence in *nmr_xray*. Nevertheless, more than 9

Table 2 Results of the clustering-I performed on the 50 best-energy conformers generated in geometric force field (*exact_xray, nmr_xray, nmr*), and performed on the 50 conformers obtained after a refinement in presence of NCS restraints (*NCS_nmr_xray, NCS_nmr*)

Conformer clustering				
Set	**Number of clusters**	**Cluster size**	**RMSD (Å) to X-ray structure**	**RMSD (Å) of the cluster**
exact_xray	6	38–45	2.2–2.3	1.5–1.8
nmr_xray	19	5–44	2.4–3.3	1.3–2.1
NCS_nmr_xray	4	41–45	2.5–2.6	1.3–1.5
nmr	33	5–21	3.7–6.8	1.5–2.4
NCS_nmr	35	5–26	3.0–7.3	1.4–2.3

Notes: The number of clusters obtained is given along with the range of cluster sizes, the range of the coordinate RMSD (Å) to the crystallographic structure 1mu4 (accuracy), and the range of the coordinate RMSD (Å) between the conformers inside each cluster (precision). The RMSD values were calculated by superimposing the backbone heavy atoms.

clusters are larger than 30 members, and the lower bounds of the RMSD are similar to those observed for *exact_xray*. The application of the NCS restraints to the *nmr_xray* conformers (*NCS_nmr_xray*), induces convergence and accuracy close to the ones observed for *exact_xray*. Indeed, the number of clusters is four and their sizes are in the range 41–45, these parameters displaying a similar order of value than in *exact_xray*. In *nmr*, a poor accuracy with respect to 1mu4 is obtained, as the coordinates RMSD to 1mu4 increased twofold with respect to other sets, the number of clusters is doubled, and the maximum cluster size is divided by two with respect to *exact_xray*. The application of NCS restraints (*NCS_nmr*) does not modify much this situation, which may be due to the relatively local symmetry applied.

The hierarchical clustering-II method, applied on clusters of conformations previously obtained, detected one group of conformers in *nmr_xray* and *NCS_nmr_xray*, and two groups in *NCS_nmr*. The following conformers sets were finally extracted from *exact_xray*, *NCS_nmr_xray* and *NCS_nmr*: (i) for *exact_xray*, the 38 best-energy conformers, (ii) for *NCS_nmr_xray*, 41 conformers obtained by clustering-I and closest to the structure 1mu4, (iii) for *NCS_nmr*, the 12-members cluster (*NCS_nmr_I*) closest to 1mu4, and a 22-members cluster (*NCS_nmr_II*), were extracted from the two groups detected by clustering-II. The four conformations sets were then refined in water and, for (ii) and (iii), in the presence of NCS restraints, to provide the sets *w_exact_xray*, *wNCS_nmr_xray*, *wNCS_nmrI* and *wNCS_nmrII*, which will be analyzed in more details below.

Conformers convergence, quality and accuracy

The Crh monomer convergence is good for all sets (Table 3), with coordinate RMSD values in the 0.6–0.9 Å range, close to the value of 0.8 Å obtained on the ssNMR structure 2rlz.[17] The small number of restraint violations larger than 0.5 Å in all clusters, along with violation RMS in the 0.11–0.15 Å range prove the good fit of the conformations to the restraints. The conformer local RMSD along the sequence (Figure 4B) qualitatively resembles to the fluctuations by residues in MD simulations (Figure 4A) and to the B factors in 1mo1 (Figure 4C), with local maxima located in the same protein regions (residues 27, 40, 57, 60, 67).

The atomic fluctuations by residues measured along the MD trajectory *sol_dimer* (data not shown) are very similar to those observed for the dimer of dimers in trajectory *sol_tetra* (Figure 4A). These two sets of fluctuations give a picture of the Crh internal dynamics in qualitative agreement with the observations made by NMR relaxation on Crh in solution.[10] Indeed, the helix α1 (residues 17–28) and the strands β2 (residues 31–37), β3 (residues 40–43)

Table 3 Quality, restraint fitting and convergence of the ARIA conformers refined in presence of NCS restraints and water (*w_exact_xray, wNCS_nmr_xray, wNCS_nmrI, wNCS_nmrII*)

Number of conformers	*w_exact_xray*	*wNCS_nmr_xray*	*wNCS_nmrI*	*wNCS_nmrII*
	38	**41**	**12**	**22**
PROCHECK core (%)	92.8 ± 2.3	92.1 ± 2.2	91.6 ± 3.4	91.0 ± 2.7
PROCHECK allowed (%)	6.8 ± 2.5	7.5 ± 2.2	7.7 ± 3.2	8.4 ± 2.9
NQACHK	–0.2 ± 0.4	–1.0 ± 0.5	–1.9 ± 0.5	–2.5 ± 0.5
RAMCHK	–3.0 ± 0.5	–3.1 ± 0.5	–1.2 ± 0.7	–2.1 ± 0.7
C12CHK	–2.2 ± 0.5	–1.9 ± 0.6	–0.7 ± 0.7	–2.1 ± 0.5
BBCCHK	0.6 ± 0.3	0.4 ± 0.3	0.7 ± 0.7	0.1 ± 0.6
INOCHK	1.0 ± 0.02	1.0 ± 0.02	0.5 ± 0.5	1.0 ± 0.03
BMPCHK	27 ± 6.6	26.2 ± 7.6	19.3 ± 4.4	46.2 ± 13.8
Number of violations ≥0.5 Å	52.0 ± 6.4	46.8 ± 6.6	19.3 ± 5.3	21.6 ± 5.5
Violation RMS (Å)	0.15 ± 1.0E-02	0.14 ± 9.0E-03	0.12 ± 1.9E-02	0.11 ± 1.7E-02
Monomer RMSD (Å)	0.6 ± 0.2	0.7 ± 0.2	0.7 ± 0.1	0.9 ± 0.2
Dimer RMSD (Å)	1.2 ± 0.4	1.1 ± 0.3	1.2 ± 0.4	1.8 ± 0.6
Monomer RMSD (Å) to 1mu4	1.0 ± 0.2	1.2 ± 0.2	1.6 ± 0.1	1.9 ± 0.2
Dimer RMSD (Å) to 1mu4	2.0 ± 0.3	2.3 ± 0.3	2.4 ± 0.4	7.6 ± 1.0
Ψ (X) (°)	–61.6 ± 15.2	–68.4 ± 11.0	–62.9 ± 15.2	–124.3 ± 34.9
Θ (Y) (°)	11.3 ± 2.2	12.4 ± 1.2	13.2 ± 2.2	9.7 ± 3.8
Φ (Z) (°)	–7.5 ± 3.1	–8.9 ± 2.3	–8.0 ± 3.4	–17.8 ± 5.3
Distance between centers of mass (Å)	20.0 ± 0.6	19.9 ± 0.5	19.4 ± 0.9	21.5 ± 0.9

Notes: Relative position of the monomers inside the dimer in the ARIA conformers is described using the angles **Ψ**, **Θ** and **Φ** (see materials and methods for definition) and the distance between the monomer centers of mass.

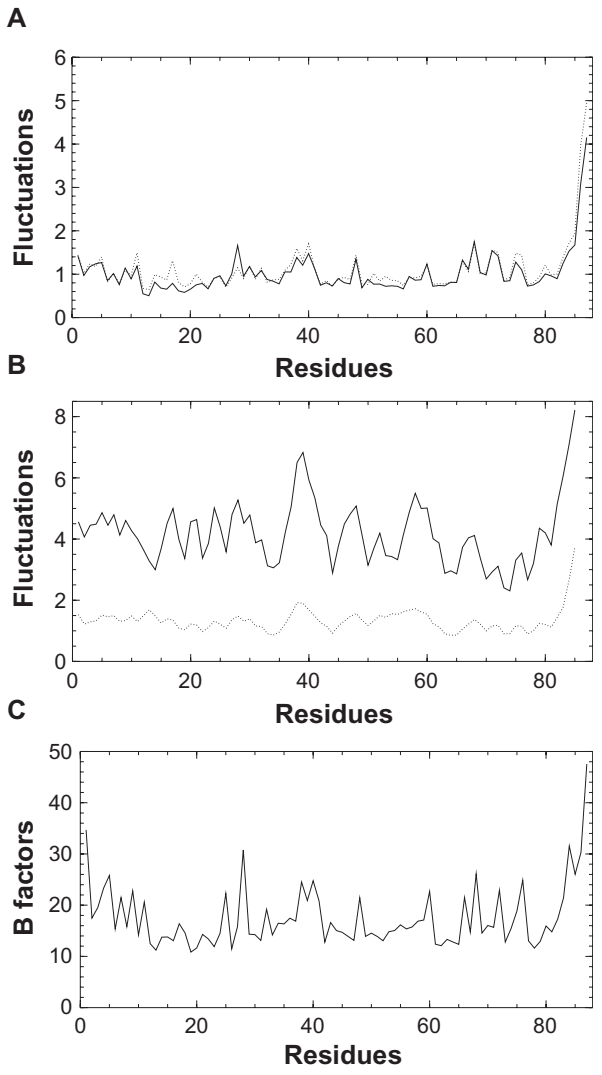

Figure 4 Comparison of the **A**) fluctuations by residues in MD simulations (*cryst_tetra*: solid, *sol_tetra*: dotted), of **B**) the mean local RMSD among ARIA conformers (geometric force field: solid, water and NCS refinements: dotted) plotted along the sequence, and of **C**) the mean B factors in the four chains of 1mo1.

and β4 (residues 60–67), which were shown to have large S2 values by NMR relaxation, display also smaller fluctuations by residues. Also, the residues 37–39 located in the turn between β2 and β3, and the residues 48–54 in helix α2, which were shown to be flexible by NMR relaxation, display larger fluctuations. On the other hand, in the simulations, the helix α3 (residues 70–80) and the strand β1 (residues 4–9) which were rigid according to NMR relaxation measurements, display more flexibility than the rigid protein regions described above.

The clustering simplifies the description of the Crh conformational landscape, with respect to the description obtained with the geometric force field. Indeed, the use of NCS restraints improves the structure precision of more than 1 Å, and the structure accuracy of about 1.0 Å for all sets except for *nmr* (data not shown). Along with clustering techniques, the NCS allows to detect sets of conformers (*w_exact_xray*, *wNCS_nmr_xray*, *wNCS_nmrI*) displaying precisions (Table 3) similar to the precision (1.3 Å) of the ssNMR structure of Crh.[17] The accuracy with respect to 1mu4, observed in all sets except *wNCS_nmrII*, compares well to the results obtained on the Crh dimer structure 2rlz calculated from ssNMR restraints,[17] for which the accuracy on the monomer is 1.6 Å, on the dimer 2.9 Å. Nevertheless, in *wNCS_nmrII*, the RMSD to 1mu4 displays a 3-fold increase.

The PROCHECK and WHATIF analyses (Table 3) determined quality parameters in the range admitted for NMR solution structures. For all runs, more than 86% of the residues are located in the core PROCHECK Ramachandran diagram. Similarly, the WHATIF parameters are in the –4/4 range, the worse values being observed for RAMCHK. The run *wNCS_nmrII* displays the worse number of interatomic bumps (BMPCHK), arising from residues mainly located in the N terminal region 1–30, which is the sign of a badly defined dimer interface. All quality parameters are constant in the four runs, which means that the application of looser restraints does not degrade the physical relevance of the generated conformations in the sets *wNCS_nmrI* and *wNCS_nmrII*.

To summarize, the lack of convergence and accuracy in the Crh dimer appears if fuzzier restraints are applied. The use of a qualitative short-range modeling of the intermolecular organization reminiscent of the crystal situation, improves drastically the dimer convergence. In the hierarchy of the restraints defining the crystal organization, the NCS restraint is thus prominent to impose the convergence toward the crystal structure, and this is an argument in favor of the early appearance of the dimer of dimers interaction in transition path from solution to crystal.

Relative monomer orientation in the dimer

The relative orientation of the monomers into the dimer was monitored (Table 3) through the Euler angles Ψ, Θ and Φ, defining the rotations around the principal inertia axes X, Y and Z (Figure 1C). The largest standard deviation is always observed for Ψ which corresponds to a largest variability around the X axis. This is in agreement with the variability in relative monomer orientation in the ssNMR structure of Crh[17] 2rlz and between the crystallographic structures 1mo1 and 1mu4 (Table 4a). In a similar way, the set of 16 dimers of dimers conformations (ens_XR) obtained from a

Table 4 Analysis of the relative position of the monomers inside the dimer: (a) in the Crh PDB structures (2rlz,[17] 1mo1, 1mu4[16]) and in the sets of 16 dimers of dimers conformers (ens_XR) obtained from the crystallographic ensemble refinement;[20] and (b) during the MD simulations (*sol_dimer, sol_tetra, cryst_tetra*)

a) PDB structures	**2rlz**	**1mo1/1mu4**	**ens_XR**
Distance (Å)	22.1 ± 0.7	21.3 ± 0.2	20.8 ± 0.1
Angle Ψ (X) (°)	–67 ± 11.6	–74.5 ± 1.8	–77.0 ± 1.6
Angle Θ (Y) (°)	12.8 ± 1.1	15.7 ± 0.6	16.0 ± 0.2
Angle Φ (Z) (°)	–7.9 ± 2.4	–11.2 ± 1.0	–12.3 ± 0.5
b) MD simulations	***sol_dimer***	***sol_tetra***	***cryst_tetra***
Distance A–B (Å)	19.2 ± 0.4	20.7 ± 0.5	20.0 ± 0.1
Distance C–D (Å)	–	20.3 ± 0.4	20.1 ± 0.2
Angle Ψ A–B (X) (°)	–77.8 ± 7.1	–80.3 ± 6.1	–79.5 ± 5.6
Angle Ψ C–D (X) (°)	–	–75.5 ± 4.8	–76.0 ± 5.0
Angle Θ A–B (Y) (°)	15.3 ± 0.8	14.2 ± 1.0	15.8 ± 1.0
Angle Θ C–D (Y) (°)	–	14.8 ± 0.8	15.6 ± 0.9
Angle Φ A–B (Z) (°)	–11.1 ± 1.8	–11.5 ± 1.5	–11.9 ± 1.9
Angle Φ C–D (Z) (°)	–	–10.3 ± 1.3	–11.2 ± 1.5

Notes: The relative position of the monomers are described through the distance between the monomer centers of mass, and through the angles **Ψ**, **Θ** and **Φ** (see materials and methods for definition).

crystallographic ensemble refinement[20] displays also Ψ as the most variable angle (Table 4a).

The lowest-energy conformer of each cluster (Figures 5B, C, D) is close to the structure 1mu4, except the lowest energy conformer of *wNCS_nmrII* (Figure 5E) which displays a difference in the relative orientation of the monomers. This difference comes from the largest bias displayed by Ψ among the orientation angles (Table 3). This feature of *wNCS_nmrII* may correspond to an orientation transiently populated during the Crh transition from solution to crystal.

During molecular dynamics (MD) simulations, larger conformational drifts are observed (data not shown) in the simulation *sol_dimer* than in the simulations *sol_tetra*, *cryst_tetra*, and the monomer RMSD are always smaller than the dimer RMSD. These two features agree well with the variability of monomer relative orientation, observed among the ARIA conformers, as well as with the drift from the X-ray crystallographic structure observed in *wNCS_nmrII*. The Euler angles stay close to the values observed in crystallographic structures (Table 4b), but again Ψ displays the largest standard deviations, in agreement with the observations made for ARIA conformers. The distance between monomer centers of mass (Table 4b) is smaller than the value observed in the crystallographic structures, and decreases along the whole *sol_dimer* simulation from 21 Å down to 19.5 Å, whereas it stays constant around 20.5 Å for simulations *sol_tetra* and *cryst_tetra*.

The relative orientation of the monomers displays the largest variability for the rotations around the longitudinal axis X of the dimer. This feature is observed for independently calculated conformations, as the sets of ARIA conformers, the ssNMR structure 2rlz, or the conformers obtained from a crystallographic ensemble refinement,[20] as well as for conformations sampled in MD simulations. This variation Ψ of may thus correspond to relative monomer orientations sampled during the transition from solution to crystal.

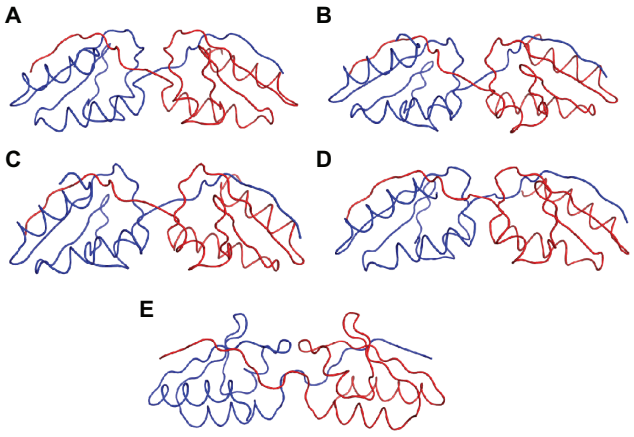

Figure 5 A) Crh dimer structure 1mu4 and lowest-energy conformers from **B**) *w_xray_exact*, **C**) *wNCS_xray_nmr*, **D**) *wNCS_nmrI* and **E**) *wNCS_nmrII*. The Crh chains are colored in blue and red. This figure was realized with pymol 0.98.[51]

Oligomer architecture

The oligomer architecture was analyzed by monitoring: the distances between secondary structure elements of the Crh

Table 5 Distances (Å) between secondary structure elements in the ARIA conformers and during the MD simulations

Secondary elements	*w_exact_xray*	*wNCS_nmr_xray*	*wNCS_nmrI*	*wNCS_nmrII*
Intra-monomer				
$\alpha 2$-$\beta 1a$	4.8 ± 0.2	5.0 ± 0.3	7.2 ± 2.5	7.2 ± 2.5
$\alpha 2$-$\beta 3$	5.7 ± 0.1	5.8 ± 0.2	5.2 ± 0.4	5.2 ± 0.4
$\alpha 3$-$\alpha 1$	9.1 ± 0.2	9.2 ± 0.2	9.5 ± 0.3	9.5 ± 0.3
$\alpha 3$-$\beta 4$	6.0 ± 0.2	6.1 ± 0.3	6.3 ± 0.2	6.3 ± 0.2
$\beta 2$-$\beta 3$	3.1 ± 0.1	3.2 ± 0.1	3.2 ± 0.1	3.2 ± 0.1
$\beta 4$-$\beta 2$	3.6 ± 0.1	3.6 ± 0.1	3.8 ± 0.1	3.8 ± 0.1
Intra-monomer				
α2-$\beta 1a$	4.8 ± 0.2	5.0 ± 0.3	7.2 ± 2.5	7.2 ± 2.5
α2-$\beta 3$	5.7 ± 0.1	5.8 ± 0.2	5.2 ± 0.4	5.2 ± 0.4
α3-$\alpha 1$	9.1 ± 0.2	9.2 ± 0.2	9.5 ± 0.3	9.5 ± 0.3
α3-$\beta 4$	6.0 ± 0.2	6.1 ± 0.3	6.3 ± 0.2	6.3 ± 0.2
$\beta 2$-$\beta 3$	3.1 ± 0.1	3.2 ± 0.1	3.2 ± 0.1	3.2 ± 0.1
$\beta 4$-$\beta 2$	3.6 ± 0.1	3.6 ± 0.1	3.8 ± 0.1	3.7 ± 0.1
Inter-monomer				
$\beta 1a$-$\beta 1a$	4.0 ± 0.1	4.0 ± 0.2	3.9 ± 0.3	3.9 ± 0.3
$\beta 1$-$\beta 4$	3.7 ± 0.2	3.6 ± 0.1	3.6 ± 0.2	3.6 ± 0.2
Secondary elements	***sol_dimer***	***sol_tetra***	***cryst_tetra***	
Intra-monomer				
α2-$\beta 1a$	3.3 ± 0.5	4.0 ± 0.2	4.4 ± 0.2	
α2-$\beta 3$	5.5 ± 0.5	5.8 ± 0.2	5.6 ± 0.2	
α3-α1	9.0 ± 0.3	9.5 ± 0.2	9.4 ± 0.3	
α3-$\beta 4$	6.0 ± 0.2	6.3 ± 0.2	6.3 ± 0.2	
$\beta 2$-$\beta 3$	3.0 ± 0.1	3.2 ± 0.2	3.4 ± 0.1	
$\beta 4$-$\beta 2$	3.1 ± 0.3	3.9 ± 0.1	3.9 ± 0.1	
Inter-monomer				
$\beta 1a$-$\beta 1a$	3.4 ± 0.5	4.0 ± 0.1	4.0 ± 0.1	
$\beta 1$-$\beta 4$	3.4 ± 0.5	4.0 ± 0.1	4.0 ± 0.1	

Notes: In the simulations, the mean values were calculated over the 2–10 ns interval and over the monomers.

dimer (Table 5), the hydrogen bonds in the secondary structure elements (df 6) and the water bridges (Figure 7).

The increase of the β4-β2, α3-β4 and α3-α1 distances in *wNCS_nmrI* and *wNCS_nmrII* (Table 5) with respect with the other ARIA conformers sets, is consistent with the disorder observed in the Crh precipitate for these secondary structure elements.[41] Beside, in the same sets, the α2-β1a distance increases and the α2-β3 distance decreases, which corresponds to α2 going apart from β1a and closer to monomer core, in agreement with the variability in the monomers orientation. During MD simulations, the distances between secondary structures (Table 5) generally increase from the dimer to the dimer of dimers architecture.

Contrary to the other distances between secondary structure elements, the distance β1a-β1a shows a tendency to decrease in ARIA conformers generated in geometric force field with looser restraints (*nmr*: data not shown) or in the MD simulation *sol_dimer* (Table 5). In the same way, the distance β1-β4 is slightly larger in *w_exact_xray*, whereas in MD simulations, the inter-monomer distance β1-β4 is larger for dimer of dimers. A modeling of the long-range crystal order thus forces the β strands involved in inter-monomer interaction to go apart.

The hydrogen bond lifetime was monitored in the secondary structures as the percentage of simulation time or of ARIA conformers for which the distance is smaller than 2.2 Å (Figure 6). Within each contact map, the hydrogen bonds in the helices are the least formed in α2 (residues 47–50), which was also shown[46] to be labile in MD simulations of HPr. Among the ARIA conformers sets, shorter lifetimes are observed in *wNCS_nmrI* (Figure 6D) and *wNCS_nmrII* (Figure 6E) than in *wNCS_nmr_xray* (Figure 6F), specially in the helices α1 (residues 17–28), α2 (residues 47–50), and between the strands β2 (residues 31–37) and β4 (residues 60–67). In MD simulations, the helices α2 and α3 are less stable in *sol_dimer* than α1 (Figure 6C), but improve their stability in *sol_tetra* (Figure 6B) and *cryst_tetra* (Figure 6A). Overall, a greater secondary structure stability is observed for conformations closer to the crystallographic structure. But, the inter-monomer hydrogen bonds between the strands β1a

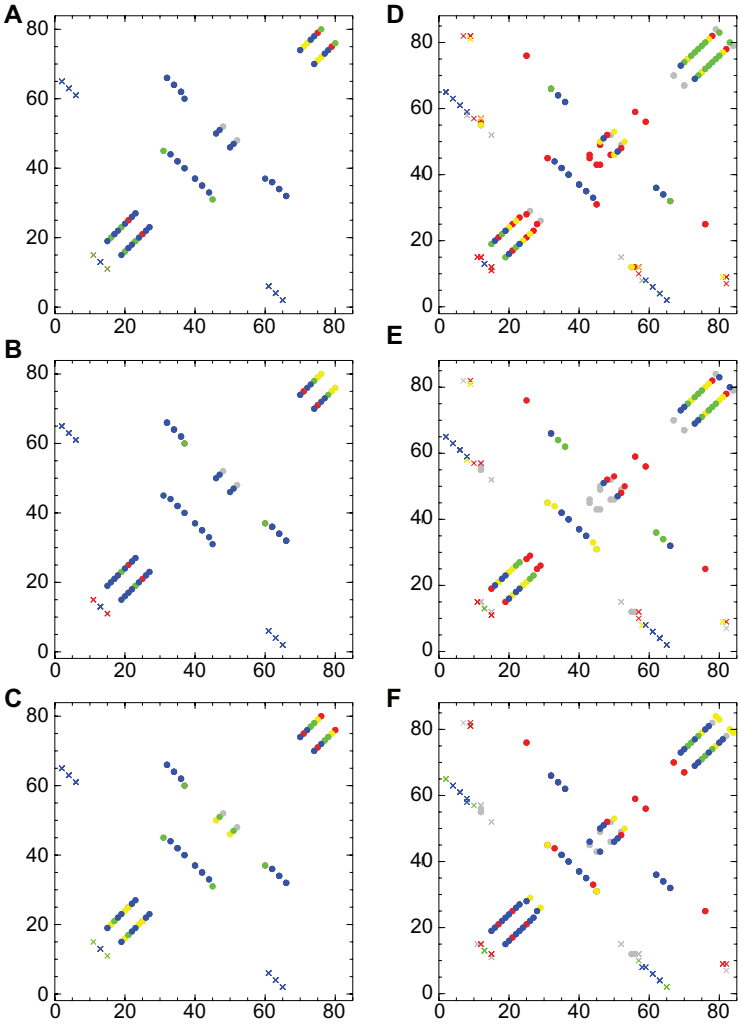

Figure 6 Contact maps showing the hydrogen bond formation along the MD trajectories or among the ARIA conformers. (a) *cryst_tetra* (chains A, B), (b) *sol_tetra* (chains A, B), (c) *sol_dimer,* (d) *wNCS_nmrI,* (e) *wNCS_nmrII,* (f) *wNCS_nmr_xray*. The percentage of hydrogen bond formation is described through color-coding: 5%–25%: red, 25%–50%: yellow, 50%–75%: green, 75%–100%: blue. Inter-monomer hydrogen bonds are marked with crosses and intra-monomer hydrogen bonds with bullets.

(residues 12–14) display the opposite pattern, as their lifetimes are shorter in *w_exact_xray* (data not shown) than in other sets of conformers, revealing thus a feature of the crystalline state. Similarly, in MD simulations, the inter-monomer hydrogen bonds between the strands β1a are more stable in *sol_dimer* than in *cryst_tetra*, in agreement with the variations of the β1a-β1a distance, described above.

The water bridges were detected in MD simulations as water molecules for which at least two atoms display a distance smaller than 2.5 Å to a protein acceptor or donor groups. Seven bridges are present in more than 25% of the molecular dynamics (MD) simulation *sol_dimer*, but this number is multiplied by 3 in the dimer of dimers simulations, where the size of the solute is multiplied by 2. The water bridges thus appear in presence of a more rigid structure and may induce this rigidity. In *sol_dimer* (Figure 7A), two water bridges are observed at the dimer interface, between O Met-51 (chain A)/H Arg-17 (chain B) and between the strands β4 and β1: H Glu-7 (chain A)/Oε1 Gln-82 (chain B). During the dimer of dimers MD simulations (*sol_tetra*, *cryst_tetra*), more water bridges are located (Figures 7B, C) between the dimers and at the monomer interfaces, and inter-monomer bridges appear between: H Ala-54/Oε1 Gln-24, O Lys-11/H Gln-15, Leu-21/Hζ3 Lys-40, H Lys-41/O Gln-24, O Met-51/H Ala-16. The appearance of water bridges is observed for MD simulations, for which the strands β1a tend to separate from each other according to the previous analyses, and may be thought to compensate for the induced structure destabilization.

The inter-molecular crystallographic water bridge between Thr-57 and Thr-12, which corresponds to a bridge conserved in the crystallographic structure,[47] is not observed

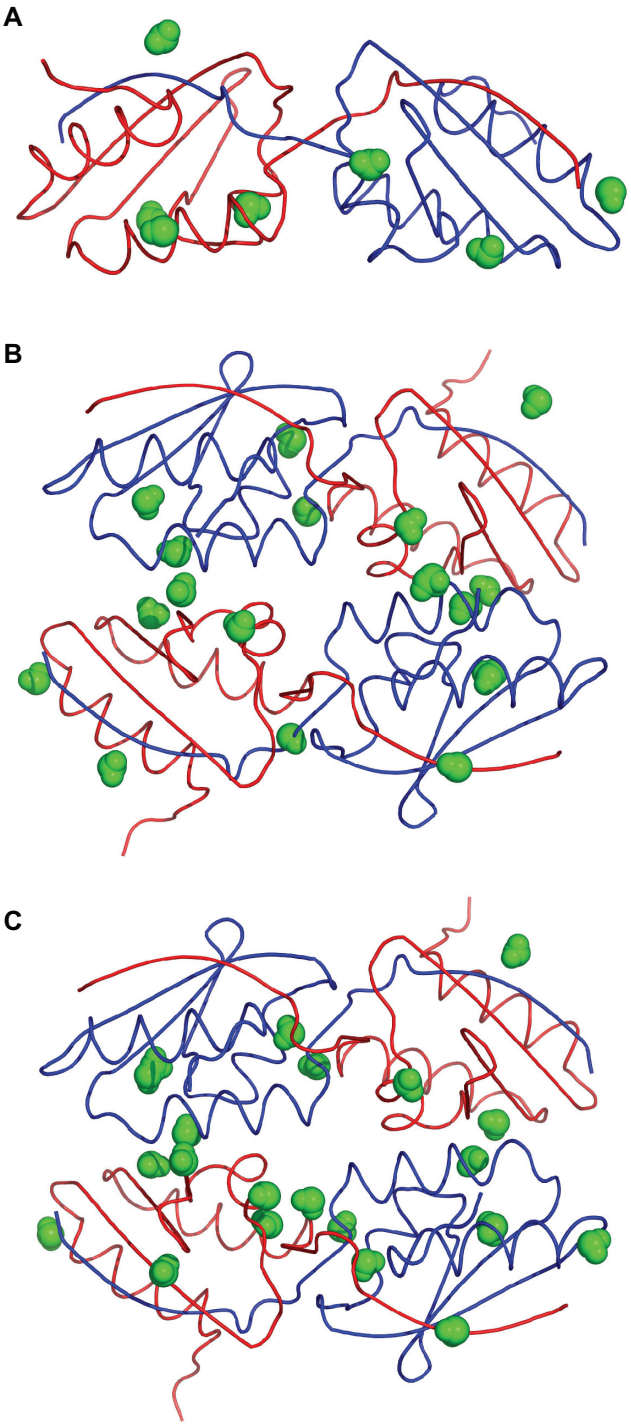

Figure 7 Water bridges observed in the MD simulations: **A**) *sol_dimer,* **B**) *sol_tetra,* **C**) *cryst_tetra*. The cuto3 distance for the detection of hydrogen bonds between water atoms and acceptor/donor groups was 2.5 Å. The Crh chains are colored in blue and red, and the water molecules are drawn in green CPK. This figure was realized with pymol 0.98.[51]

in any of the MD simulations. In *cryst_tetra*, the crystallographic water positions are not observed, and this may be the consequence of not modeling the exact environment and packing of the crystal. On the other hand, the disappearance of the Thr-57/Thr-12 bridge in MD simulations is correlated with a larger variability of the relative monomer orientation than in the crystallographic ensemble refinement, and supports the importance of this bridge for stabilizing the dimeric structure, in agreement with the observation of Lesage et al.[47] Indeed, the position of the Thr-57/Thr-12 bridge is appropriate to block the rotation around the axis X, which is responsible for the largest part of the variability in monomers orientation inside the dimer.

To summarize, the Crh conformations closest to the crystal structure, are characterized by more stable intra-monomer secondary structures along with a paradoxical separation of the β1a strands. This separation is accompanied by the apparition of a larger number of water bridges stabilizing the oligomer architecture. In that respect, the absence in MD simulations of water bridges present in the crystal is probably a reason for the residual variability in the monomers relative orientation.

Discussion conclusion

Several structure calculations were performed using ARIA with sets of distance restraints based on the solution and solid-state NMR experiments, as well as on the crystallographic structures. The clustering of solutions and the use of environment restraints (NCS, water) allows to generate dimer conformations exhibiting precision and accuracy similar to the ones observed for the ssNMR structure of the Crh dimer.[17] The approach proposed here makes full profit of the data recorded in solution, which are easier accessible than ssNMR data, and of ssNMR chemical shifts which can be nowadays obtained even for proteins of up to 100 amino acids.[48] The information about intermolecular restraints were here partly obtained from the X-ray crystallographic structure, but, as methodology for the measurement of restraints is advancing at a fast pace,[49] one can expect in the future to rely more on the ssNMR information.

The sampled conformations give insights into the relative orientation of monomers during the transition from solution to crystal, as in *wNCS_nmrII*. The inclusion of specific water molecules at the interfaces was already shown to be important in the prediction of complex structures.[50] Here, the presence of water molecules allows the apparition of water bridges stabilizing the inter-molecular interactions.

The variability of monomer orientation is concentrated in rotations around the dimer longitudinal axis, and this is just amplified but not created by the use of fuzzy NMR distance restraints, as this feature is observed also in a set of crystallographic conformers obtained from ensemble refinement along the structure factors. More generally,

the comparable pattern of observed orientations for all series of conformations supports a funnel shape of the conformational space during the transition from solution to crystal.

Acknowledgments/Disclosures

Benjamin Bardiaux thanks the European Union Grant SPINE (QLG2-CT-2002-00988) and the "Ministère de l'Enseignement Supérieur" for the financial support in the frame of the ACI IMPBio (project ICMD-RMN). The authors thank the ACI IMP-Bio (ICMD RMN), the CNRS, the Agence Nationale pour la Recherche (JC05_44957 and ANR-07-PCVI-0013-03) and the Institut Pasteur for funding. Thérèse Malliavin thanks Dr Levin for providing the CNS 1.2 script files required for crystallographic ensemble refinement.

Abbreviations

NMR, Nuclear Magnetic Resonance; ssNMR, solid-state NMR; Crh, Catabolite repression HPr-like protein; RMSD, root-mean square deviation; RMSF, root-mean square fluctuations; NCS, non-crystallographic symmetry.

References

1. Park S, Mrse A, Nevzorov A, et al. Three-dimensional structure of the channel-forming trans-membrane domain of virus protein "u" (Vpu) from HIV-1. *J Mol Biol*. 2003;332:409–424.
2. Roszak A, Howard T, Southall J, et al. Crystal structure of the RC-LH1 core complex from Rhodopseudomonas palustris. *Science*. 2003;302:1969–1972.
3. Andronesi O, Becker S, Seidel K, Heise H, Young H, Baldus M. Determination of membrane protein structure and dynamics by magic-angle-spinning solid-state NMR spectroscopy. *J Am Chem Soc*. 2005;127:12965–12974.
4. Wider RRG, Billeter M, Hornemann S, Glockshuber R, Wiithrich K. Prion protein NMR structure and familial human spongiform encephalopathies. *Proc Natl Acad Sci U S A*. 1998;95:11667–11672.
5. Wasmer C, Lange A, Melckebeke HV, Siemer A, Riek R, Meier B. Amyloid fibrils of the HET-s(218–289) prion form a beta solenoid with a triangular hydrophobic core. *Science*. 2008;319:1523–1526.
6. Helmus J, Surewicz K, Nadaud P, Surewicz W, Jaroniec C. Molecular conformation and dynamics of the Y145Stop variant of human prion protein in amyloid fibrils. *Proc Natl Acad Sci U S A*. 2008;105:6284–6289.
7. Bousset L, Redeker V, Decottignies P, Dubois S, Marchal PL, Melki R. Structural characterization of the fibrillar form of the yeast Saccharomyces cerevisiae prion Ure2p. *Biochemistry*. 2004;43:5022–5032.
8. Jehle S, van Rossum B, Stout J, et al. αB crystallin: a hydrid solid-solution state NMR investigation reveals structural aspects of the heterogeneous oligomer. *J Mol Biol*. 2009;385:1481–1497.
9. Traaseth N, Shi L, Verardi R, Mullen D, Barany G, Veglia G. Structure and topology of monomeric phospholamban in lipid membranes determined by a hybrid solution and solid-state NMR approach. *PNAS*. 2009;106:10165–10170.
10. Favier A, Brutscher B, Blackledge M, et al. Solution structure and dynamics of Crh, the Bacillus subtilis catabolite repression HPr. *J Mol Biol*. 2002;317:131–144.
11. Azuaga A, Neira J, van Nuland N. HPr as a model protein in structure, interaction, folding and stability studies. *Protein Pept Lett*. 2005;12:123–137.
12. Kalbitzer H, Hengstenberg W. The solution structure of the histidine-containing protein (HPr) from Staphylococcus aureus as determined by two-dimensional 1H-NMR spectroscopy. *Eur J Biochem*. 1993;216:205–214.
13. van Nuland N, Hangyi I, van Schaik R, et al. The high-resolution structure of the histidine-containing phosphocarrier protein HPr from Escherichia coli determined by restrained molecular dynamics from nuclear magnetic resonance nuclear Overhauser effect data. *J Mol Biol*. 1994;237:544–559.
14. Hahmann M, Maurer T, Lorenz M, Hengstenberg W, Glaser S, Kalbitzer H. Structural studies of histidine-containing phosphocarrier protein from Enterococcus fae-calis. *Eur J Biochem*. 1998;252:51–58.
15. Penin F, Favier A, Montserret R, et al. Evidence for a dimerisation state of the Bacillus subtilis catabolite repression HPr-like protein, Crh. *J Mol Microbiol Biotechnol*. 2001;3:429–432.
16. Juy M, Penin F, Favier A, et al. Dimerization of Crh by reversible 3D domain swapping induces structural adjustments to its monomeric homologue HPr. *J Mol Biol*. 2003;332:767–776.
17. Loquet A, Bardiaux B, Gardiennet C, et al. 3D Structure Determination of the Crh Protein from Highly Ambiguous Solid-State NMR Restraints. *J Am Chem Soc*. 2008;130:3579–3589.
18. Schmidt H, Sperling L, Gao Y, et al. Crystal polymorphism of protein GB1 examined by solid-state NMR spectroscopy and X-ray diffraction. *J Phys Chem B*. 2007;111:14362–14369.
19. Rieping W, Habeck M, Bardiaux B, Bernard A, Malliavin T, Nilges M. ARIA2: automated NOE assignment and data integration in NMR structure calculation. *Bioinformatics*. 2007;23:381–382.
20. Levin E, Kondrashov D, Wesenberg G, Phillips G. Ensemble refinement of protein crystal structures: validation and application. *Structure*. 2007;15:1040–1052.
21. Böckmann A, Lange A, Galinier A, et al. Solid state NMR sequential resonance assignments and conformational analysis of the 2x10.4 kDa dimeric form of the Bacillus subtilis protein Crh. *J Biomol NMR*. 2003;27:323–329.
22. Ulrich L, Akutsu H, Doreleijers J, et al. BioMagResBank. *Nuc Acids Res*. 2007;36:D402–D408.
23. Etzkorn M, Böckmann A, Lange A, Baldus M. Probing molecular interfaces using 2D magic-angle-spinning NMR on protein mixtures with different uniform labeling. *J Am Chem Soc*. 2004;126:14746–14751.
24. Cornilescu G, Delaglio F, Bax A. Protein backbone angle restraints from searching a database for chemical shift and sequence homology. *J Biomol NMR*. 1999;13:289–302.
25. Nilges M. A calculation strategy for the structure determination of symmetric dimers by 1H. *Proteins*. 1993;17:297–309.
26. Linge J, Williams M, Spronk C, Bonvin A, Nilges M. Refinement of protein structures in explicit solvent. *Proteins*. 2003;50:496–506.
27. Nederveen A, Doreleijers J, Vranken W, et al. Recoord: a recalculated coordinates database of 500+ proteins from the pdb using restraints from the biomagresbank. *Proteins*. 2005;59:662–672.
28. Fossi M, Oschkinat H, Nilges M, Ball L. Quantitative study of the effects of chemical shift tolerances and rates of SA cooling on structure calculation from automatically assigned NOE data. *J Magn Reson*. 2005;175:92–102.
29. Brunger A. Version 1.2 of the Crystallography and NMR system. *Nat Protoc*. 2007;2:2728–2733.
30. Bardiaux B, Bernard A, Rieping W, Habeck M, Malliavin T, Nilges M. Influence of different assignment conditions on the determination of symmetric homodimeric structures with ARIA. *Proteins*. 2009;75:569–585.
31. Laskowski R, MacArthur M, Moss D, Thornton J. Procheck: a program to check the stereochemical quality of protein structure. *J Appl Cryst*. 1993;26:283–291.
32. Hooft R, Vriend G, Sander C, Abola E. Errors in protein structures. *Nature*. 1996;381:272–272.

33. Dominguez C, Boelens R, Bonvin A. HADDOCK: a protein-protein docking approach based on biochemical or biophysical information. *J Am Chem Soc*. 2003;125:1731–1737.
34. Gordon A. *Classification*. London Chapman and Hall/CRC, 1999.
35. Walser R, Hunenberger P, van Gunsteren W. Molecular dynamics simulations of a double unit cell in a protein crystal: volume relaxation at constant pressure and correlation of motions between the two unit cells. *Proteins*. 2002;48:327–340.
36. Case D, Darden T, Cheatham T, et al. *AMBER 9*, 2004.
37. Hornak V, Abel R, Okur A, Strockbine B, Roitberg A, Simmerling C. Comparison of multiple Amber force fields and development of improved protein backbone parameters. *Proteins*. 2006;65:712–725.
38. Darden T, York D, Pedersen L. Particle mesh Ewald: An N.log(N) method for Ewald sums in large systems. *J Chem Phys*. 1993;98:10089–10092.
39. Ryckaert J, Ciccotti G, Berendsen H. Numerical integration of the cartesian equations of motion of a system with constraints: molecular dynamics of n-alkanes. *J Comput Phys*. 1977;23:327–341.
40. Loncharich R, Brooks B, Pastor R. Langevin dynamics of peptides: the frictional dependence of isomerization rates of N-acetylalanyl-N'-methylamide. *Biopolymers*. 1992;32:523–535.
41. Etzkorn M, Böckmann A, Penin F, Riedel D, Baldus M. Characterization of folding intermediates of a domain-swapped protein by solid-state NMR spectroscopy. *J Am Chem Soc*. 2007;129:169–175.
42. Fay N, Redeker V, Savistchenko J, Dubois S, Bousset L, Melki R. Structure of the prion Ure2p in protein fibrils assembled in vitro. *J Biol Chem*. 2005;280:37149–37158.
43. Ranson N, Stromer T, Bousset L, Melki R, Serpell L. Insights into the architecture of the Ure2p yeast protein assemblies from helical twisted fibrils. *Protein Sci*. 2006;15:2481–2487.
44. Paci E, Gsponer J, Salvetella X, Vendruscolo M. Molecular dynamics studies of the process of amyloid aggregation of peptide fragments of transthyretin. *J Mol Biol*. 2004;340:555–569.
45. Cecchini M, Curcio R, Pappalardo M, Melki R, Caflisch A. A molecular dynamics approach to the structural characterization of amyloid aggregation. *J Mol Biol*. 2006;357:1306–1321.
46. Canalia M, Malliavin T, Kremer W, Kalbitzer H. Molecular dynamics simulations of HPr under hydrostatic pressure. *Biopolymers*. 2004; 74:377–388.
47. Lesage A, Emsley L, Penin F, Böckmann A. Investigation of dipolar-mediated water-protein interactions in microcrystallune Crh by solid-state NMR spectroscopy. *J Am Chem Soc*. 2006;128: 8246–8255.
48. Pintacuda G, Giraud N, Pierattelli R, Böckmann A, Bertini I, Emsley L. Solid-State NMR of a Paramagnetic Protein: Assignment and Study of the Human Dimeric Oxidized Zn(II)-Cu(II) Superoxide Dismutase (SOD). *Angew Chem Int Ed Engl*. 2006;46: 1079–1082.
49. Lewandowski J, Paepe GD, Griffn R. Proton assisted insensitive nuclei cross polarization. *J Am Chem Soc*. 2007;129:728–729.
50. van Dijk A, Bonvin A. Solvated docking: introducing water into the modelling of biomolecular complexes. *Bioinformatics*. 2006;22:2340–2347.
51. DeLano W. The PyMOL Molecular Graphics System. httpwwwpymolorg 2002.
52. Bond C. TopDraw: a sketchpad for protein structure topology cartoons. *Bioinformatics*. 2003;19:311–312.